

$$K(x) = \pi \cdot 10^{-10} \cdot \left[\frac{2\pi I_0}{x}, m^*(x) \right], \quad (4)$$

$$x = \log_{10}, \quad (5)$$

where $e(x)$ is an arbitrary function except for some condition on the magnitude of $e(x)$, and

$$k(x) + e(x) = \int_{x_0}^x K(x)f(x)dx, \quad (2)$$

Eq. (1) becomes Eq. (1), we introduce an error term in Eq. (1). Then the numerical solution of the integral equation such as the techniques developed by Phillips and Twomey for the technique of numerical solvability solving the Fredholm integral equation, Phillips and Twomey have developed a technique index is close to unity.

Eq. (1) is used, the forward matrix approximation to Eq. (1) is

Some $k(x)$ is not known accurately, if the straight

of a particle.

scatterring cross section to the geometrical cross section

$m^*(x)$ is the index of refraction, and Q is the ratio of the

particles per cubic centimeter in the interval $x_i + dx$,

where x_i is the particle radius, $n(x)$ is the number of

particles by aerosol particles, which is given by

evaluates the extinction takes place, one can

wavelengths, where no absorption taking at several

From the attenuation measurements at several

and Twomey were applied to the present inverse prob-

lem.

In this paper, the techniques developed by Phillips

little meterology by Flemming and Wark,¹²

fully to solve the so-called inverse problem of the satel-

II. Method

A method of evaluating the aerosol size distribution from the spectral attenuation measurements is shown. The process consists of solving the simultaneous integral equations, and examples are given of solutions based on the attenuation measurements made by Knechtel et al. over the Chesapeake Bay. It is found that the evaluated individual size distributions do not necessarily follow the power law, although departures from it are mostly small. If the power law is to be adopted neglecting small departures, the evaluated results are in average expressed by $r^{-1.6}$, where r is the radius of aerosols. In this study, the evaluated relative index of aerosols is assumed to be 1.6, and some discussion is made of the effect of adopting a different refractive index value on estimation of the size distribution.

The authors are with the Geophysical Institute, Tohoku University, Sendai, Japan.
Received August 19, 1968.
Technical Editor, Philip D. Morrison, Jr., has developed a simple technique of determining the refractive index of an aerosol by Van de Hulst.⁸ This formula, which was originally developed by Twomey¹⁰ for the efficiency factor of the Air Force, is valid when the value of the refractive index n is close to unity. These results were applied successfully to the first kind and thus obtained general solution of the Fredholm integral equation of numerically solvability solving the Fredholm integral equation, Phillips and Twomey have developed a simple technique index is close to unity.

Attenuation

Yamamoto and Masayuki Tanaka

Determination of Aerosol Size Distribution from Spectral Attenuation Measurements

$$f(x) = 10^{4x} n(10^x). \quad (5)$$

With respect to the condition for $\mathcal{E}(\lambda)$, we assume

$$\sum_{\lambda} \mathcal{E}^2(\lambda) = \text{const.} \quad (6)$$

The indicial function $f(x)$ of the integral Eq. (2) becomes constant in the case of the Junge distribution. It is, therefore, expected that in most cases, which occur in the atmosphere, $f(x)$ will not change much with x . This property of $f(x)$ will make the determination of it easier than that of $n(r)$ in the original Eq. (1). The Eq. (2) no longer has a unique solution. In order to pick a meaningful solution out of the family of solutions satisfying Eqs. (2) and (6), a further constraint given by

$$\int_{x_s}^{x_l} \left(\frac{d^2 f_s}{dx^2} \right)^2 dx = \min_{f \in \mathcal{F}} \int_{x_s}^{x_l} \left(\frac{d^2 f}{dx^2} \right)^2 dx, \quad (7)$$

is introduced by Phillips, and an alternative one given by

$$\int_{x_s}^{x_l} (f_t - f_s)^2 dx = \min_{f \in \mathcal{F}} \int_{x_s}^{x_l} (f_t - f)^2 dx, \quad (8)$$

is proposed by Twomey. Here, f_s is the solution and f_t is a trial solution, or a gross *a priori* estimate of the solution and \mathcal{F} means a family of solutions.

In order to solve the problem numerically, we divide the interval into N parts and replace the integral equation by an equivalent linear system. The solution which satisfies Eqs. (2), (6), and (7) is given by

$$\mathbf{f} = (\mathbf{A}^T \mathbf{A} + \gamma \mathbf{H})^{-1} \mathbf{A}^T \mathbf{k}, \quad (9)$$

and the solution satisfying Eqs. (2), (6), and (8) is

$$\mathbf{f} = (\mathbf{A}^T \mathbf{A} + \gamma \mathbf{I})^{-1} (\mathbf{A}^T \mathbf{k} + \gamma \mathbf{f}_t), \quad (10)$$

where \mathbf{f} is the solution vector, \mathbf{A} is the matrix whose elements are defined by the coefficients of the equivalent linear system of Eq. (2), \mathbf{A}^T is the transpose of \mathbf{A} , γ is an arbitrary parameter introduced as a Lagrangean multiplier, \mathbf{H} is the smoothing matrix, \mathbf{I} is the identity matrix, \mathbf{k} is the input vector or that of observed extinction coefficients, and \mathbf{f}_t is the vector of the trial solution. In these solutions γ , which is an arbitrary non-negative parameter, controls the amount of smoothing. The solution with $\gamma = 0$ corresponds to the direct solution of Eq. (2), and increasing γ produces greater smoothing. There exists a certain range of values of γ in which the solutions are not affected significantly by the values of γ . A value of γ is to be chosen from this range, and once it is chosen, the same value of γ is to be used throughout the study.

In this study, the solution of Eq. (9) was first obtained by approximating $f(x)$ by a step function. In this case, the elements of the matrix \mathbf{A} is given by

$$A_{ij} = \int_{x_j}^{x_{j+1}} K(\lambda_i, x) dx, \quad (i, j = 1, 2, \dots, N), \quad (11)$$

and for a quadrature of equal division, the smoothing matrix is given by Twomey to be

$$\mathbf{H} = \begin{bmatrix} 1 & -2 & 1 & 0 & 0 \\ -2 & 5 & -4 & 1 & 0 & 0 \\ 1 & -4 & 6 & -4 & 1 & 0 \\ 0 & 1 & -4 & 6 & -4 & 1 & 0 \\ & & & & & & \\ 0 & 1 & -4 & 5 & -2 & & \\ 0 & 1 & -2 & 1 & & & \end{bmatrix}. \quad (12)$$

Then using this solution as the trial solution \mathbf{f}_t , the second solution was obtained from Eq. (10). In this case, the function $f(x)$ was approximated by the connection of line segments passing through the centers of steps. Then the components of the vector \mathbf{f} or \mathbf{f}_t are given by $f_j = a_j (j = 1, 2, \dots, N-1)$ and $f_N = b_{N-1}$, where a_j is the slope of the j segment and b_{N-1} is the intercept of the last segment, and the elements of the matrix \mathbf{A} are expressed as follows:

$$A_{ij} = \int_{x_i}^{x_{j+1}} K(\lambda_i, x) dx + x_j \int_{x_i}^{x_j} K(\lambda_i, x) dx - x_{j+1} \times \int_{x_i}^{x_{j+1}} K(\lambda_i, x) dx, \quad (i = 1, 2, \dots, N, j = 1, 2, \dots, N-2) \quad (13)$$

$$A_{i,N-1} = \int_{x_{N-1}}^{x_N} K(\lambda_i, x) dx + x_{N-1} \int_{x_1}^{x_{N-1}} K(\lambda_i, x) dx, \quad (i = 1, 2, \dots, N) \quad (14)$$

$$A_{i,N} = \int_{x_1}^{x_N} K(\lambda_i, x) dx, \quad (i = 1, 2, \dots, N). \quad (15)$$

III. Refractive Index of Aerosols and Kernel Function

In order to compute the kernel function $K(\lambda, x)$ Eq. (2), it is necessary to know the value of refractive index m^* . According to Gebbie *et al.*¹³ and Simola, natural haze is approximately transparent in visible near ir regions, and the refractive index of haze in these regions lies somewhere between 1.33 and 1.54, the former value corresponds to that of water droplets and the latter one, to that of NaCl. Gibbons¹⁵ indicates that, for values of the size parameter $\alpha = 2\pi r/a$ from 3 to about 6.5, the refractive index of 1.33 approximates natural haze more adequately than other values while from the analysis of the scattering function measurements in the visible region, Voltz¹⁶ has shown that the refractive index of aerosol particles is about 1.3. Recently, from a comparison between computed and measured values of the elliptical polarization of light scattered by aerosols, Eiden¹⁷ has found that for dry aerosols, a real part of refractive index is 1.50 and the imaginary part of it is between 0.01 and 0.1. He has found that for moist aerosols, both the real and imaginary parts decrease. In this study, we tentatively assume that the natural aerosol particles are homogeneous dielectric spheres of refractive index $m^* = 1.50$ in wavelength region from 0.35 μ to 2.27 μ . In order to supplement the assumption for the values of refractive

Fig. 1. Wei

index, some effect of change evaluation

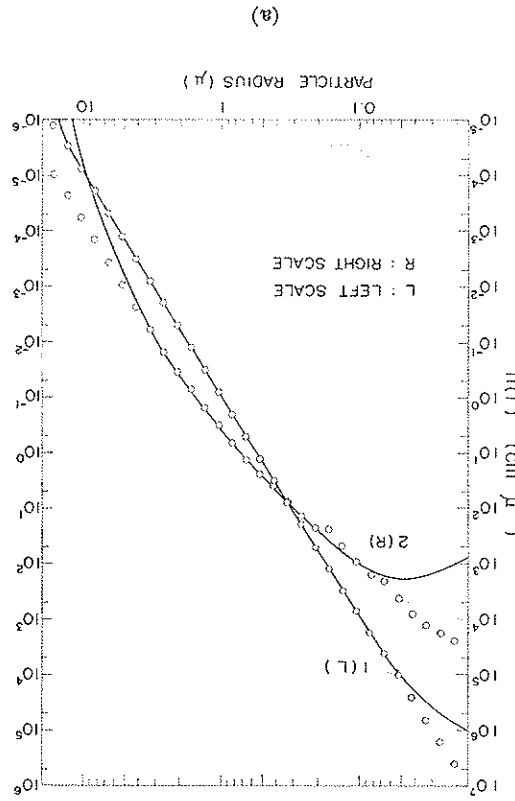
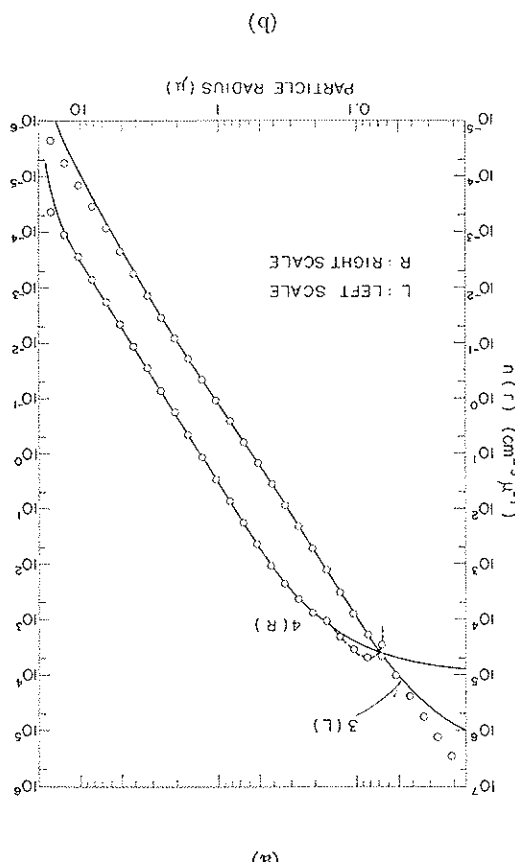
The value kernel function show the wavelength filtering are were used as to make tends to 2 μ .

IV. Model

Before See II to carried out accuracy of distribution coefficient at the the calculated from Eq. a trial sol correspond used. 0.3 2.27 μ , and calculation

The results in Figs. 2 particle radius solid line

Fig. 2. (a) Comparison of the assumed model size distribution and estimated one. Solid line shows the model size distribution and white or black circles, estimated one. (b) Same as Fig. 2(a), but for different models.

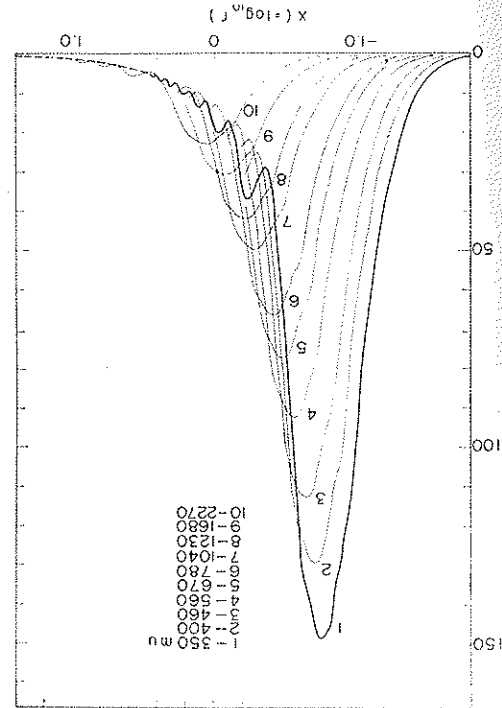


The results of the numerical experiments are shown in Figs. 2(a) and 2(b), where abscissa indicates the particle radius in μ and ordinate $n(r)$ in $\text{cm}^{-3} \mu^{-1}$. The solid line in the figures expresses the assumed model built for different models. The radius in μ , where $n(r)$ is obtained through the calculation of the numerical experiments, are used: 0.35μ , 0.46μ , 0.56μ , 0.78μ , 1.23μ , 1.68μ , and 2.27μ , and the value of γ adopted is 0.05 throughout the calculation. The following seven wavelength values are used: 0.35μ , 0.46μ , 0.56μ , 0.78μ , 1.23μ , 1.68μ , and 2.27μ . This size distribution is determined from Eq. (8)], and a corresponding solution of boundary's constraint [Eq. (10)], and a trial solution of boundary's constraint [Eq. (9)]. The size distribution is then determined from Eq. (8)], the size distribution is determined upon the calculated $k(\lambda)$, the size distribution is determined at each wavelength concerned, and basing upon distribution of aerosols, calculate the extinction coefficient κ of the method. To do so, we assume a size uncertainty of the method. The broken line in the figure is drawn so as to make accurate with the fact that the value of κ tends to 2 for large values of the size parameter $a = 2\pi/\lambda$.

Before applying the present method described in Sec. II to the actual attenuation measurements, we carried out some numerical experiments to check the accuracy of the method. To do so, we assume a size distribution of the aerosols, calculate the extinction coefficient κ as a parameter. The values of κ are tabulated by Penndorf's formulae area coefficient Q tabulated by scattering wavelength λ as a parameter. The values of κ , taking the kernel function K given by Eq. (4). In Fig. 1 are shown the kernel functions as a function of λ , taking the kernel function of m^* being assumed, we can calculate the distribution of the aerosol size distribution.

The value of m^* being assumed, we can calculate the final result of calculating the value of refractive index on the final effect of changing the value of refractive index on the final kernel function K given by Eq. (4). In Fig. 1 are shown the kernel functions as a function of λ , taking the kernel function of m^* being assumed, we can calculate the distribution of the aerosol size distribution.

Fig. 1. Weighting function $K(\lambda, \alpha)$, vs $\alpha = \log_{10}$ for various wavelengths.



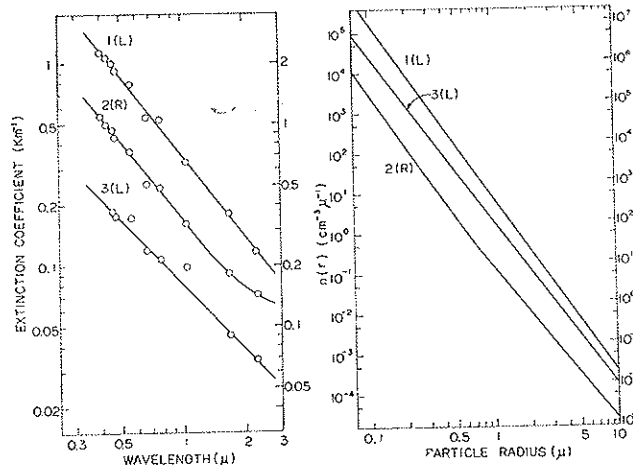


Fig. 3. Observed extinction coefficient and estimated size distribution. The curve marked by L (or R) should be referred to the ordinate scaled on the left (or right) side of the figure. Curves 1, 2, and 3 are based on observations on 13 January, 13:45, 11:10, and 21 April, respectively.

distribution and the white or black circles express the reproduced distribution as the results of calculation. The letter L or R attached to the number of the curve represents the scale of the ordinate to be used. Curve 1 indicates a typical Junge distribution, 2, a Woodcock distribution, which is known to represent the distribution in a maritime air mass, 3, an approximate Junge distribution in which some deviation from the r^{-4} law is observed in the region of $r < 0.5 \mu$, and 4 gives the overlapped distribution of 1 and 2.

From the results of these numerical experiments, it is found that the size distribution can be reproduced or determined fairly well in the range $0.1 \mu < r < 5 \mu$. Some errors of estimation are seen outside of the region. This is because very small or large particles are ineffective to lights in the visible and near ir region, as can be seen from Fig. 1.

V. Determination of Aerosol Size Distribution from Attenuation Measurements

The method described in the preceding sections is applied to the spectra attenuation measurements made by Knestrick *et al.*¹⁹ over the Chesapeake Bay along the horizontal distances of 5.5 km or 16.3 km. The observations were carried out between April 1959 and January 1960, and the results of thirty-six observations are reported. We have carried out estimation of the size distribution for all of them. However, in order to make the description brief, we classify the results of observations into five types according to the shape of $k(\lambda)$, and examples for each type are shown.

Figure 3 shows the results for the cases in which the extinction coefficient follows or nearly follows the power law. The observed extinction coefficient is shown in the left figure and the evaluated size distribution, in the right figure. In these figures double scales are again used in the ordinate to avoid overlapping of curves. The extinction coefficient for the curves 1 and 3 follows

the power law $\lambda^{-1.3}$ and $\lambda^{-1.1}$, respectively, and correspondingly, the size distribution for the curve 1 and 3 follows $n^{-4.3}$ and $n^{-4.1}$, respectively. In curve 2, some deviation from the power law is seen. In the observations by Knestrick *et al.*, such cases as shown in Fig. 3 in which the extinction coefficient and accordingly size distribution obey the power law were unexpectedly few (only four cases out of thirty-six). This might be due to the fact that the observations by Knestrick *et al.* covered rather a wider spectral range extending to near ir. On the other hand, the power law for the extinction coefficient originally deduced by Ångström²⁰ is based on observations in the visible region, and also many cases that deviate from the power law for the aerosol size distribution are already known to exist as described in the introduction.

Figure 4 shows the cases in which extinction coefficient decreases rapidly with increase of wavelength. Correspondingly, particle concentration decreases rap-

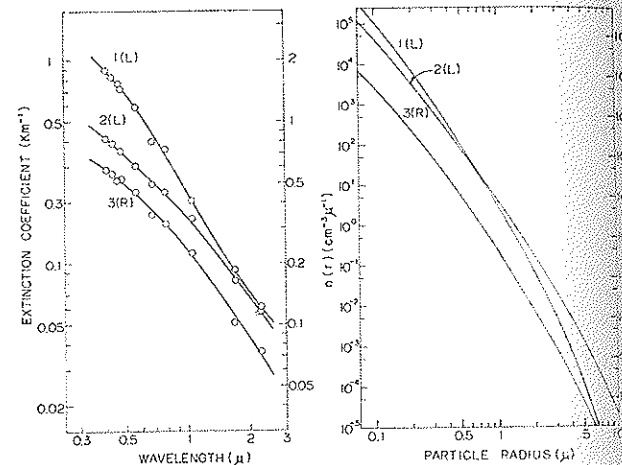


Fig. 4. Same as Fig. 3, except that curves 1, 2, and 3 are based on observations on 13 January, 14:40, 29 April, 13:00 and 11:00, respectively.

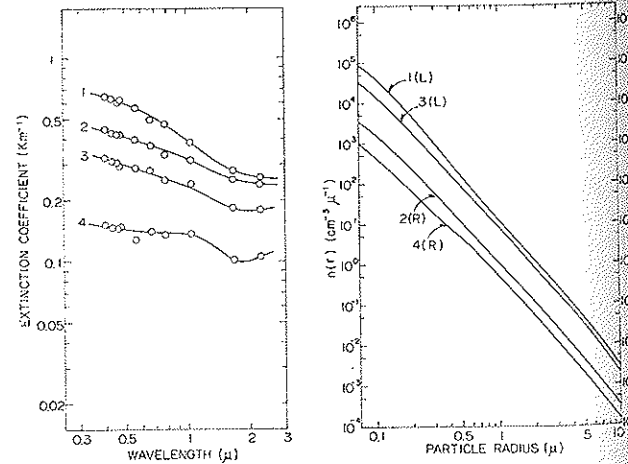
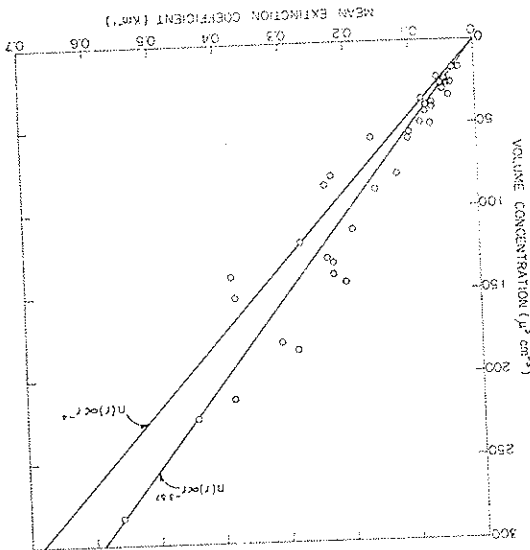


Fig. 5. Same as Fig. 3, except that curves 1, 2, 3, and 4 are based on observations on 29 April, 29 September, 08:25, 29 September, 08:10 and 08:50, 5 January, respectively.

Fig. 8. Volume concentration vs mean extinction coefficient. White circles are due to observations and estimations, while the straight lines represent the relation for aerosols obeying the power law, $\tau = k \cdot r^{-3/2}$ and $\tau = k \cdot r^{-1}$, respectively.



where $\lambda_1 = 0.35 \mu$ and $\lambda_2 = 2.27 \mu$. The white circles in the figure are based on measurements by Kneserick et al. Scattering of points in the figure corresponds to a mean extinction coefficient,

$$\frac{1}{\lambda_2 - \lambda_1} \int_{\lambda_1}^{\lambda_2} k(\lambda) d\lambda,$$

Figure 8 shows the relation between the volume concentration in the radius range, $0.1 \mu \leq r \leq 5 \mu$, and the mean extinction coefficient,

$$V_r = \frac{4\pi}{3} \int_{\infty}^{\infty} r^3 n(r) dr,$$

where

$$\int_{\infty}^{\infty} k(\lambda) d\lambda = \frac{3}{2} \pi V_r \int_{\infty}^{\infty} Q(\lambda) \lambda^{-2} d\lambda, \quad (17)$$

from Eq. (1), $k(\lambda)$ is known over a whole spectral range, we have mean extinction coefficient over a limited spectral range than a simple $k(\lambda)$. Because in an ideal case in which and it is expected that V_r is more reasonably related to a size range. This quantity V_r is given by

$$V_r = \frac{3}{4} \pi \int_{\infty}^{\infty} r^3 n(r) dr, \quad (18)$$

From the estimated size distribution, we can also estimate mate the volume concentration of aerosols in a limited size range.

VI. Volume Concentration and Mean Extinction Coefficient

In the right figure, suggesting predominance of larger particles. These cases are not necessarily unusual in Kneserick et al., observations are more than ten cases are found out of thirty-six cases.

Figure 7 shows the cases in which the extinction coefficient curve has minimum at 1.68μ and then grows as the wavelength increases. Corresponding size distribution curves are rather complicated as shown in Figure 7.

Figure 6 shows the cases in which the extinction coefficient curve of the size distribution curve is also con-

tinuous, the slope of the size distribution curve is seen in the right to the preceding cases. As can be seen in the right

extinction coefficient curve is concave upward, contrary extinction 6 shows the cases in which the slope of the

Woodcock distribution occurring in the maritime air mass. Nine cases out of thirty-six belong to this group.

Figure 2 in curve 2 in Fig. 2(a), which represents the similarity to curve 2 in Fig. 2. These size distributions have those in Figs. 3 and 4. The extinction coefficient is very slow. Corresponding size distributions, which are shown in the right figure, indicate slower slope than

shown. Figure 5 shows the cases in which decrease of extinction coefficient with increase of wavelength is very slow.

Figure 4 shows the cases in which decrease of extinction coefficient with increase of wavelength is very slow.

Figure 4 shows the cases in which decrease of extinction coefficient with increase of particle size as shown in the right figure of Fig. 4.

Figure 4 shows the cases in which decrease of extinction coefficient with increase of particle size as shown in the right figure of Fig. 4.

Figure 4 shows the cases in which decrease of extinction coefficient with increase of particle size as shown in the right figure of Fig. 4.

Figure 4 shows the cases in which decrease of extinction coefficient with increase of particle size as shown in the right figure of Fig. 4.

Figure 4 shows the cases in which decrease of extinction coefficient with increase of particle size as shown in the right figure of Fig. 4.

Figure 4 shows the cases in which decrease of extinction coefficient with increase of particle size as shown in the right figure of Fig. 4.

Figure 4 shows the cases in which decrease of extinction coefficient with increase of particle size as shown in the right figure of Fig. 4.

Figure 4 shows the cases in which decrease of extinction coefficient with increase of particle size as shown in the right figure of Fig. 4.

Figure 4 shows the cases in which decrease of extinction coefficient with increase of particle size as shown in the right figure of Fig. 4.

Figure 4 shows the cases in which decrease of extinction coefficient with increase of particle size as shown in the right figure of Fig. 4.

Figure 4 shows the cases in which decrease of extinction coefficient with increase of particle size as shown in the right figure of Fig. 4.

Figure 4 shows the cases in which decrease of extinction coefficient with increase of particle size as shown in the right figure of Fig. 4.

Figure 4 shows the cases in which decrease of extinction coefficient with increase of particle size as shown in the right figure of Fig. 4.

Figure 4 shows the cases in which decrease of extinction coefficient with increase of particle size as shown in the right figure of Fig. 4.

Figure 4 shows the cases in which decrease of extinction coefficient with increase of particle size as shown in the right figure of Fig. 4.

Figure 4 shows the cases in which decrease of extinction coefficient with increase of particle size as shown in the right figure of Fig. 4.

Figure 4 shows the cases in which decrease of extinction coefficient with increase of particle size as shown in the right figure of Fig. 4.

Figure 4 shows the cases in which decrease of extinction coefficient with increase of particle size as shown in the right figure of Fig. 4.

Figure 4 shows the cases in which decrease of extinction coefficient with increase of particle size as shown in the right figure of Fig. 4.

Figure 4 shows the cases in which decrease of extinction coefficient with increase of particle size as shown in the right figure of Fig. 4.

Figure 4 shows the cases in which decrease of extinction coefficient with increase of particle size as shown in the right figure of Fig. 4.

Figure 4 shows the cases in which decrease of extinction coefficient with increase of particle size as shown in the right figure of Fig. 4.

Figure 4 shows the cases in which decrease of extinction coefficient with increase of particle size as shown in the right figure of Fig. 4.

Figure 4 shows the cases in which decrease of extinction coefficient with increase of particle size as shown in the right figure of Fig. 4.

Figure 4 shows the cases in which decrease of extinction coefficient with increase of particle size as shown in the right figure of Fig. 4.

Figure 4 shows the cases in which decrease of extinction coefficient with increase of particle size as shown in the right figure of Fig. 4.

Figure 4 shows the cases in which decrease of extinction coefficient with increase of particle size as shown in the right figure of Fig. 4.

Table I Conversion Factors A and A' for Various Values of m^* and ν

ν	m^*	1.50	1.486	1.44	1.40	1.33
3.7	A	1.0	1.02	1.09	1.16	1.32
	A'	1.0	1.02	1.09	1.17	1.34
	percent error	0	0	0	0.9	1.5
4.0	A	1.0	1.03	1.12	1.22	1.45
	A'	1.0	1.03	1.14	1.25	1.52
	percent error	0	0	1.8	2.5	4.8
4.3	A	1.0	1.04	1.15	1.27	1.58
	A'	1.0	1.04	1.18	1.34	1.72
	percent error	0	0	2.6	5.5	10.1
4.5	A	1.0	1.04	1.17	1.31	1.66
	A'	1.0	1.04	1.21	1.40	1.87
	percent error	0	0	3.4	6.9	12.7

variety of behaviors of the observed extinction coefficients and estimated size distributions as shown in the preceding section. In spite of such variety of behaviors departures from the power law in the evaluated size distributions were mostly small. Therefore, it would be of interest to know a governing power law in the case of Knestrick *et al.* measurements, if departures from it are to be neglected. To investigate this, we assume a power law given by

$$n(r) = cr^{-\nu}. \quad (19)$$

Then, from Eqs. (1) and (16), we have

$$\frac{1}{\lambda_2 - \lambda_1} \int_{\lambda_1}^{\lambda_2} k(\lambda) d\lambda / V = \frac{3(2)^{\nu-5} \pi^{\nu-3}}{\lambda_2 - \lambda_1} \int_0^\infty Q(\alpha, m^*) \alpha^{2-\nu} d\alpha \frac{\int_{\lambda_1}^{\lambda_2} \alpha^{3-\nu} d\alpha}{\int_{r_1}^{r_2} r^{3-\nu} dr}. \quad (20)$$

Thus, if we fix λ_1 , λ_2 , r_1 , and r_2 , the ratio of the mean extinction coefficient to V depends on ν . In Fig. 8, two straight lines: one corresponding to $\nu = 3.57$ (least-squares fit to all the data) and the other, to $\nu = 4$ (Junge distribution) are shown. From the figure, it can be seen that Knestrick *et al.* measurements are in average expressed by the power law $n(r) \propto r^{-3.57}$. Taking into account that the observations are made over the Chesapeake Bay, this result may be interpreted as representing the feature of the aerosol size distribution near sea surface. However, it should be noticed that estimation of number of large particles is predominantly dependent upon the extinction coefficient at 1.68μ and 2.27μ in the present method. Whereas, because of existence of near ir absorption bands of H_2O and CO_2 around these spectral regions, deduction of the extinction coefficient at these wavelengths is likely to be less accurate than that at visible regions. Therefore, in order to examine validity of the present result, it is desirable to have more observations.

VII. Effect of Refractive Index on the Present Method of Estimating the Size Distribution

In the present investigation, we have assumed $m^* = 1.50$. Some ambiguity remains on this choice of the refractive index value. Therefore, we consider how estimation of the size distribution change if another value be used for m^* .

We first consider the case in which the size distribution follows the power law, as given by Eq. (19). Corresponding extinction coefficient $k(\lambda)$ is given by

$$k(\lambda) = 2^{\nu-3} \pi^{\nu-2} \lambda^{3-\nu} C(m^*) \int_0^\infty Q(\alpha, m^*) \alpha^{2-\nu} d\alpha, \quad (21)$$

where the size parameter, $\alpha = 2\pi r/\lambda$ is used as variable in the integral. Substituting $m^* = 1.50$ in Eq. (21) and equating the formula to Eq. (21), we have

$$C(m^*) = C(1.50) \frac{\int_0^\infty Q(\alpha, 1.50) \alpha^{2-\nu} d\alpha}{\int_0^\infty Q(\alpha, m^*) \alpha^{2-\nu} d\alpha}. \quad (22)$$

The numerical value of the conversion factor $A = \int_0^\infty Q(\alpha, 1.50) \alpha^{2-\nu} d\alpha / \int_0^\infty Q(\alpha, m^*) \alpha^{2-\nu} d\alpha$ is listed in Table I for several values of m^* and ν , which are likely to occur in the atmosphere.

Next, we consider the case of a more general size distribution. As has been shown by Van de Hulst,⁸ when m^* is close to unity, the scattering area coefficient Q is approximately, but uniquely, expressed by the normalized size parameter $\rho = 2\alpha(m^*-1)$. According to Penndorf,¹⁸ this approximation is fairly well applicable to natural aerosols whose refractive index lies in between 1.33 and 1.5. Introducing a new variable t given by

$$t = r(m^*-1), \quad (23)$$

we have

$$Q\left(\frac{2\pi t}{\lambda(m^*-1)}, m^*\right) = Q^*\left(\frac{2\pi t}{\lambda}\right), \quad (24)$$

where, according to Van de Hulst, Q^* is approximately independent of m^* . Referring to Eqs. (23) and (24), the extinction coefficient $k(\lambda)$ is given by

$$k(\lambda) = \int_0^\infty \pi t^2 Q^*\left(\frac{2\pi t}{\lambda}\right) g(t) dt, \quad (25)$$

where

$$g(t) = \frac{1}{(m^*-1)^3} n\left(\frac{t}{m^*-1}\right). \quad (26)$$

Substituting $m^* = 1.50$ in Eq. (26), and equating the formula to Eq. (26), we have

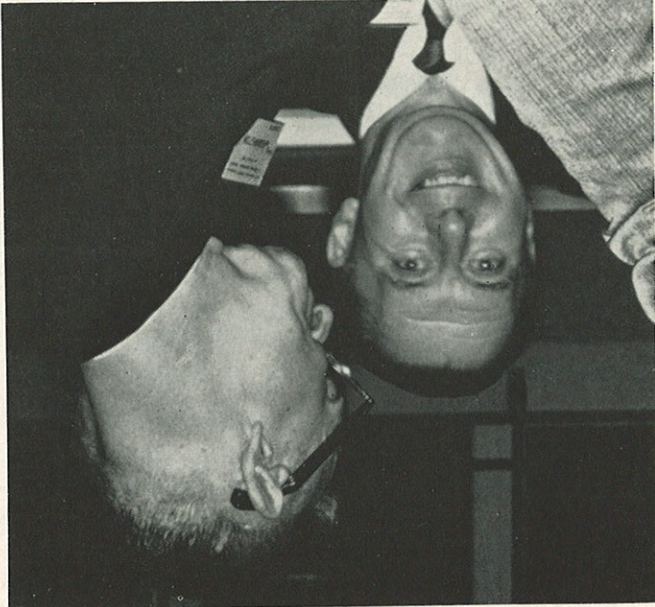
$$n\left(\frac{0.5}{m^*-1} R\right) = \left(\frac{m^*-1}{0.5}\right) n(R), \quad (27)$$

where $R = t/0.5$. This formula can be interpreted as follows. The number of aerosols at radius $0.5R/(m^*-1)$ in the case of $m^* = m^*$ is equal to $[(m^*-1)/$

Meeting.

R. Norman Jones National Research Council of Canada (left) and Guy Waddington Office of Critical Tables during the CODATA

photo WINC



20. A. Ansgstrom, Georg. Ann. II, 156 (1929).
 Amer. 52, 1010 (1962).
 19. G. L. Kneserle, T. H. Colesden, and J. A. Currie, J. Opt. Soc. Amer. 56-204 (6).
 18. R. Penndorf, Geophys. Res. Papers No. 45 [AFRC-TR-17, R. Eiden, Appl. Opt. 5, 569 (1966)].
 16. F. E. Vold, Bear. Deutsch. Meteorol. 2, No. 13, 47 (1954).
 15. M. G. Gibbons, J. Opt. Soc. Amer. 48, 172 (1958).
 14. D. Simclair, in *Proceedings of the U.S. Technical Conference on Air Pollution* (McGraw-Hill Book Company, Inc., New York, 1952), Chap. 18.
 13. H. A. Gebbie, W. R. Hardinge, C. Hillsman, A. W. Pryce, and (1966).
 12. D. Q. Warke and H. E. Flemming, Mon. Weather Rev. 94, 351
 11. S. Twomey, J. Franklin Inst. 279, 95 (1965).
 10. S. Twomey, J. Ass. Comp. Mach. 10, 97 (1963).
 9. D. L. Phillips, J. Ass. Comp. Mach. 9, 84 (1962).
 Wiley & Sons, Inc., New York, 1957).
 8. H. C. Van de Hulst, *Light Scattering by Small Particles* (John (1963).
 7. K. S. Shifrin and A. Ya. Perelman, Opt. Spektros. 15, 484 (1963).
 6. K. S. Shifrin and A. Ya. Perelman, Opt. Spektros. 15, 362 (1963).
 5. K. S. Shifrin and A. Ya. Perelman, Opt. Spektros. 15, 285
 4. R. G. Elmidge, J. Atmos. Sci. 23, 605 (1966).
 3. R. G. Elmidge, J. Meteorol. 14, 55 (1957).
 2. J. A. Currie, J. Opt. Soc. Amer. 51, 548 (1961).
 1. C. Junge, J. Meteorol. 12, 13 (1955).

References

This work was supported by the Environment Seine Services Administration under a contract.

The numerical values of the approximate conversion factor $A_* = [0.5/(m^*-1)]^{-\frac{1}{m^*-1}}$ and of its present error from A is also listed in Table I. As we have taken the case of $m^* = 1.50$ as standard, it is natural that the present error increases when the value of m^* departs from 1.50. The present error also increases with increase of ν , or when small particles predominate. This fact suggests that use of the Van de Hulst parameter ν is not necessary enough for the determination of number of small particles, or, in other words, for the representation of ϕ around its first maximum against

$$C(m^*) = \left(\frac{0.5}{0.5 - 1} \right)^{\nu - 1} C(1.50) \quad (30)$$

$$\alpha = (2\pi/\lambda)(= p/2). \quad (29)$$

(28)

$$f(\lambda) = 2^{\nu - 3} \nu^{-2} (m^* - 1)^{-3} C(m^*) \lambda^{3 - \nu} \times \int_0^\infty \phi_*(\lambda) e^{-2 - \nu d \lambda} \quad (27)$$

We again return to the simple power law case, and assume the Van de Hulst approximation. By substitu-

tion of Eq. (19) into Eq. (25), we have

values of m^* . We again return to the simple size distribution is made by assuming $m^* = 1.50$, the result can be used in estimating the size distribution for other cases of $m^* = 1.50$. Thus, once the estimation of size distribution is made by assuming $m^* = 1.50$, the result can be used in estimating the size distribution for other cases of $m^* = 1.50$. Thus, once the estimation of size

Determination of Aerosol Size Distributions from Spectral Attenuation Measurements

H. Grassl

An iteration method for the determination of size distributions of aerosols from spectral attenuation data similar to the one previously published for clouds, is presented. The basis for this iteration is to consider the extinction efficiency factor of particles as a set of weighting functions covering the entire radius region of a distribution. The weighting functions were calculated exactly from the Mie theory. Aerosol distributions are shown derived from tests with analytical size distributions and also generated from measured aerosol extinction data in seven spectral channels from $0.4\text{-}\mu$ to $10\text{-}\mu$ wavelength in continental aerosols. The influence of relative humidity on the complex index of refraction is also discussed.

Introduction

After a previous successful attempt to determine cloud drop size distributions from spectral transmission measurements by an iteration method¹, this method is being used to derive size distributions of aerosols. First, the iteration method is tested on analytical size distributions representing mean distributions for continental and maritime aerosols. Then two size distributions are presented that have been generated by inversion of our own measurements of the extinction coefficient on 2 days in continental aerosols. The multichannel spectroradiometer that was used for these measurements in the $0.4\text{-}10\text{-}\mu$ wavelength region has already been described in Ref. 1.

There are some publications²⁻⁴ that also show possibilities for the determination of aerosol size distributions from spectral attenuation measurements. However, these methods required *a priori* assumptions about the nature of the distributions and the kernel of the integral equation to be solved. The iteration method described here needs no assumptions about the kernel and the distributions.

Iteration Method

The volume extinction coefficient k_λ of spherical polydispersions, like cloud particles and aerosols in general at the wavelength λ , can be written:

$$k_\lambda = \pi \int_{r_1}^{r_2} Q(r, \lambda) \cdot n(r) \cdot r^2 \cdot dr \quad (1)$$

where

$$Q(r, \lambda),$$

the extinction efficiency factor depends on the particle radius r and wavelength λ . Values for

$$Q(r, \lambda)$$

were calculated exactly from Mie theory using a regression method given by Plass⁵; $n(r)$ is the particle concentration per volume and per unit of radius, and r_1 and r_2 bracket the size distribution. Inversion of the above integral equation for $n(r)$ is achieved by an iteration method. The basis of the iteration is the following property of scattering and absorbing particles.

The extinction efficiency factor

$$Q(r, \lambda)$$

as a function of r (Fig. 1) reaches, for a fixed wavelength (channel of the spectroradiometer) and corresponding value of the refractive index, a series of pronounced maxima for certain radius regions. The first maximum value with increasing r is also the absolute maximum. Therefore, these curves can be called weighting functions for the function $r^2 \cdot n(r)$. The following iteration procedure makes use of this property. For simplification we assume that the extinction in a wavelength channel is only caused by particles from the radius interval that corresponds to the maximum of the associated weighting function.

We assume $n_0(r)$ to be the initial size distribution. The extinction coefficient k_{0i} for all channels is calculated for the extinction coefficient compared to the initial distribution in the radius interval that corresponds to the maximum of the associated weighting function.

The author is with Institut für Meteorologie, Universität Mainz, 65 Mainz, Postfach 3980, Germany.

Received 21 May 1971.



Fig. 1. Extinction efficiency factor versus particle radius in microns.

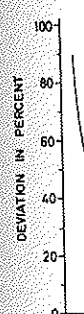


Fig. 2. Deviation in percent versus particle radius in microns.

lated for the extinction coefficient compared to the initial distribution in the radius interval that corresponds to the maximum of the associated weighting function.

For the final iteration step, $n(r)$ equals $n_0(r)$ plus a correction term calculated by quadrature.

with the imaginary part of the refractive index.

$$Q(r, \lambda)$$

Fig. 3. Variation of the extinction efficiency

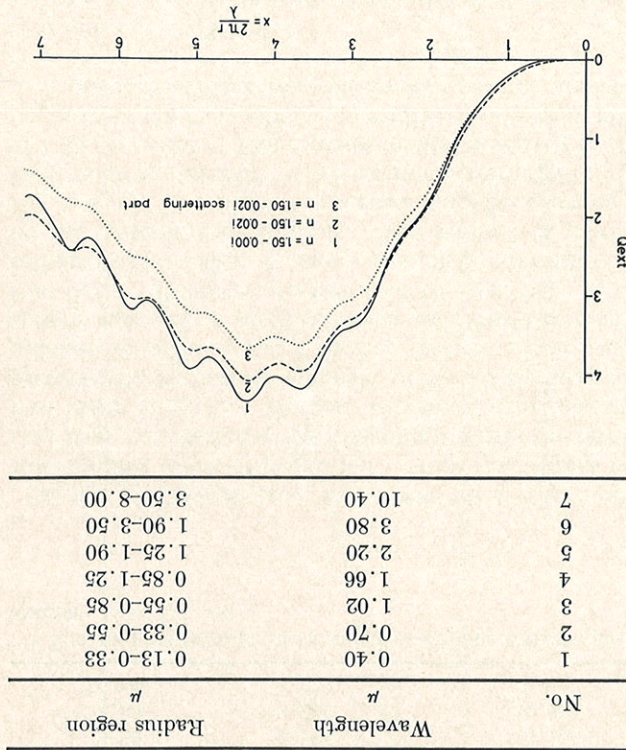
Table I. Channels and Associated Radius Regions (μ)

Table I shows the peak wavelengths of the radiometer channels and the associated radii of the wave lengths of the 0.5- μ and 10- μ wave lengths. The value of the refractive index between 0.5- μ and 10- μ wavelength is only a slight variation in the refractive index constituents shown up to 10 μ , because the major constituents show up to 10 μ and others. The real part holds also in the intermediate and others, and the real part was proposed by Yamamoto² and others, and the real part was polluted areas of Germany, and the real part by Finschke⁶ in heavily polluted areas of Germany, and the real part was measured by Finschke⁶ in heavily polluted areas of the intermediate part was measured by 1.50-0.02. The value of the intermediate part was measured by 1.50-0.02. The value of the intermediate part was chosen to be complex channels and the associated radii regions, the radiometer channels did not affect the convergence.

Figure 2 shows the initial distribution. Even setting $n_0(r) =$ constant did not affect the convergence. The curve at the extreme left for 10.4 μ reaches a maximum at about 6- μ radius. The extinction efficiency depending on radius for different wavelength. The curve at the extreme left for 10.4 μ reaches a maximum at about 6- μ radius.

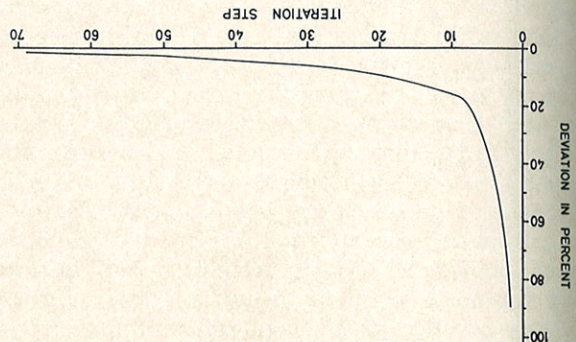
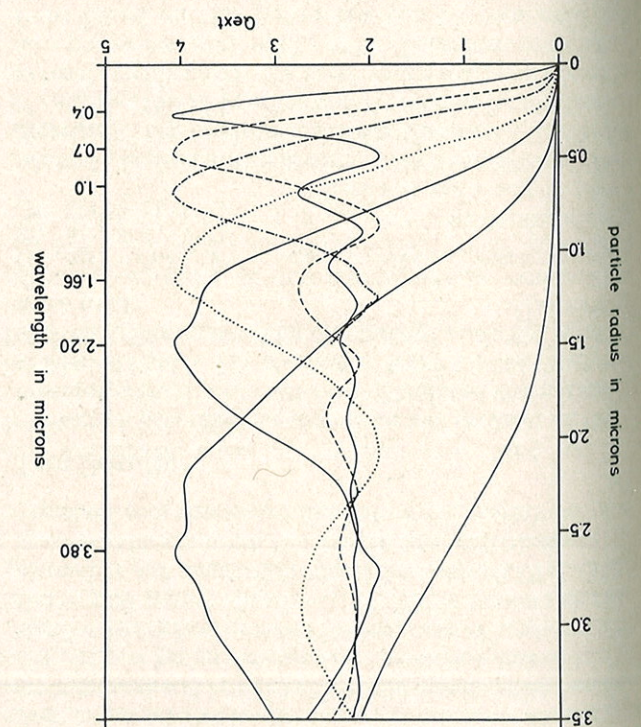
For the following examples the number of channels, m , equals seven. The mean value of radius, \bar{r} , is calculated by quadrature interpolation in the corresponding interval.

$$n_1(f_i) = (k_i/k_0) n_0(f_i) \quad i = 1, m. \quad (2)$$

is varied.

$$Q(r, \lambda)$$

in the radius region with the maximum of the radius distribution, and corresponds to the distribution paralel to the calculated extinction coefficient k_i of the estimated coefficient k_i of channel i will now be compared for this distribution from Eq. (1). The measured extinction distribution $n(r) = 5.33 \cdot 10^4 \cdot r \cdot \exp(-8.94/r)$.

Fig. 2. Convergence of the iteration for maritime aerosols with a size distribution $n(r) = 5.33 \cdot 10^4 \cdot r \cdot \exp(-8.94/r)$.Fig. 1. Extinction efficiency depending on radius for different wavelength. The curve at the extreme left for 10.4 μ reaches a maximum at about 6- μ radius.

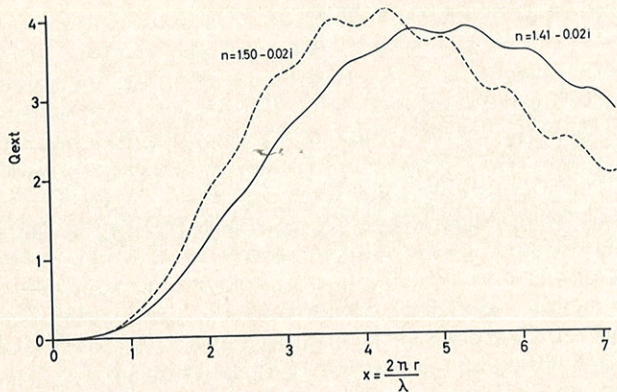


Fig. 4. Variation of the extinction efficiency

$Q(r, \lambda)$
with the real part of the refractive index.

Table II. Extinction Coefficients for Maritime and Continental Aerosol Size Distributions^a

Wavelength (μ)	Extinction coefficient distribution 1 (cm ⁻¹)	Extinction coefficient distribution 2 (relative units)
0.40	0.995×10^{-6}	0.575
0.70	1.046	0.455
1.02	1.049	0.345
1.66	0.913	0.214
2.20	0.744	0.155
3.80	0.385	0.085
10.40	0.052	0.027

^a The analytic form of these size distributions corresponds to numbers 1 and 2 in text.

In our Mie calculations we allowed for a variation of the complex index of refraction. Only little effect was seen from a variation of the imaginary part of the refractive index (Fig. 3). We can, therefore, conclude that possible absorption by aerosols, although perhaps significant for calculations of the heat balance of the atmosphere, has only a small influence on aerosol transmission data. However, variation of the real part of the refractive index (Fig. 4) shows a much greater influence on the extinction of aerosols. The value 1.41 used in Fig. 4 would be realistic for aerosol particles growing at 95% relative humidity if we assume a refractive index of 1.33 for water. The measurements presented in this paper were made at relative humidities lower than 80% in those layers containing the major part of aerosols, thus avoiding a correction of the real part of the refractive index.

For a successful iteration, the existence of radiometer channels at the lower and upper end of the size distribution is necessary. Only then can an exact value of the extinction coefficient k_λ be determined. If the radiometer channel corresponding to the lowest radius region

does not reach the lower end of the size distribution, the error caused will be tolerable if the size distribution does not show a further increase in particle number toward smaller particles, because the extinction increases with the second power of radius. As Table I shows the iteration does not account for particles below 0.13 μ. There is also evidence that the power law distributions will break off at a particle radius below a 0.1-μ radius.

Test Results

Prior to inverting measured aerosol extinction, the iteration method was tested on calculated extinction coefficients (Table II) generated from known analytical size distributions. The following size distributions were used:

- (1) $n(r) = 5.33 \cdot 10^4 \cdot r \cdot \exp(-8.994\sqrt{r})$ maritime aerosol
- (2) $n(r) = C_1 \cdot r^{-4}$ continental aerosols,
- (3) $n(r) = C_2 \cdot r^{-3}$

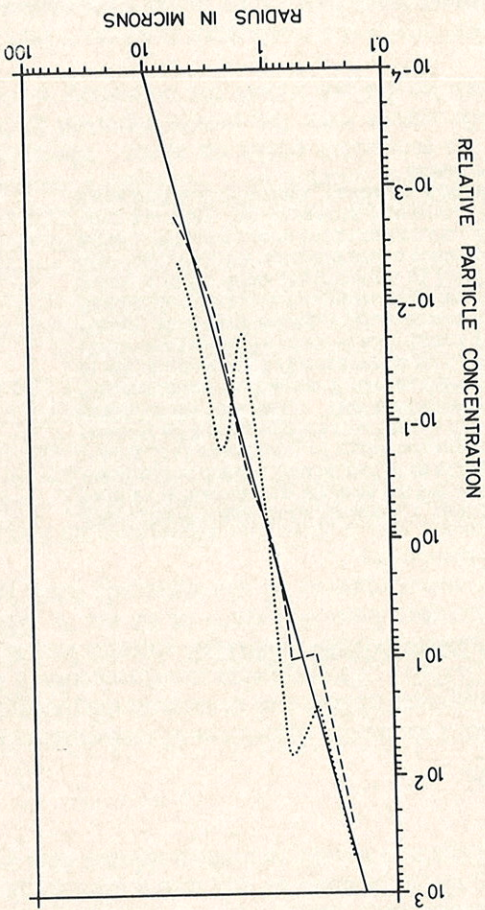
where C_1 and C_2 are constants. As was stated by Deirmendjian,⁷ the analytical distribution $n(r) = 4.97 \cdot 10^6 \cdot r^2 \cdot \exp(-15.1186\sqrt{r})$ proposed by him for continental aerosols yields nearly the same single scattering function as a power law $n(r) = C_1 \cdot r^{-4}$. Therefore, our calculations based on this power law can be compared with those using Deirmendjian's distribution.

The iteration method approximates the size distributions so well (Fig. 5) that the sum over all deviations of the iterated from the calculated extinction coefficients of all channels is always smaller than 1%. The stability of this inversion technique has already been tested in Ref. 1 by addition of random errors to the extinction coefficients. These errors result in an increasing deviation from the distribution iterated with exact values of extinction, but they do not influence the convergence. Addition of great errors of 5% rms results in increasing variations of the size distribution, and the iteration converges to a size distribution the summed deviation of which is also increasing. This means that there is no aerosol distribution that leads to the set of extinction coefficients with added great errors. This interdependence of different channels is caused by the high non-zero value of the weighting functions for big particles. If the entire radius region, including the upper and lower end of the size distribution, is covered by channels of the spectroradiometer, the inversion seems unique, since the desired size distribution was approximated in all tests with calculated extinction coefficients.

Results of an Inversion of Measured Transmission Data

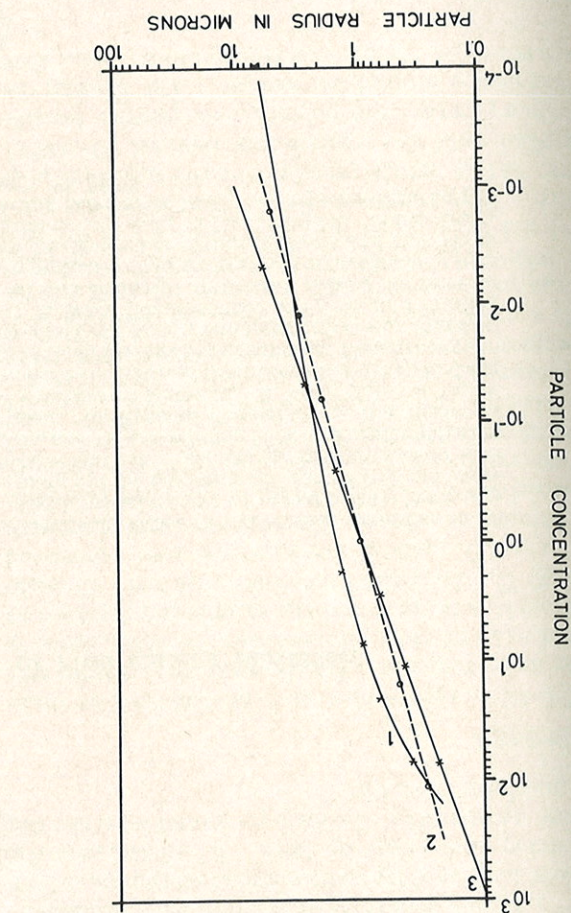
The spectral extinction coefficients k_λ for aerosols cannot be determined immediately from spectral atmospheric transmission measurements using the sun as a light source. The measured value A of one channel is proportional to $\exp(-u)$, where u is the optical depth of a slant path in the atmosphere. Extinction by air molecules, water vapor, ozone, carbon dioxide, and other minor constituents of the atmosphere contributes to the optical depth. All these contributions should be eliminated to get the aerosol extinction. The ozone and

Fig. 6. Size distributions achieved by inversion of measured extinction coefficients for continental aerosols. The dashed curve shows the size distribution following a power law with $n(r) = C_1 \cdot r^{-4}$. Numbers at the crosses correspond to the listed size distributions. Figures 1 and 3 show the association of iterated and exact size distributions.



curve shows the iterated curve.

Circles represent the analytically size distribution, and the dashed curves 1 and 3 the crosses are the calculated size distributions, at curve numbers at the crosses correspond to the listed size distributions.



Channel	k_a	$n(r)$	k_a	$n(r)$	12 October 1970	16 October 1970
1	0.169	246	0.0520	485		
2	0.152	93	0.0512	25.4		
3	0.1169	93	0.0510	65.3		
4	0.0821	10.2	0.0330	1.02		
5	0.0623	1.02	0.0225	0.0179		
6	0.0300	0.0016	0.0134	0.183		
7	0.0210	0.00174	0.0045	0.004		

Table III. Measured Aerosol Extinction Coefficients k_a per Air Mass and Associated Size Distributions $n(r)$ in Relative Units Generated by Inversion of the Extinction Coefficient k_a from other moleculer extinction coefficients were taken from tables published by Ellermann.⁸ Water vapor and carbon dioxide were corrected for by using transmission data from Lundich, Germany, about 30 km from the measurement site. At a $3.8-\mu$ wavelength the influence of a pressure gradient were derived from radiosonde data from tables from Watt et al.⁹ The values of water vapor content were determined from data from a water vapor monitor Wytat et al.⁹ The influence of nitrogen was also accounted for. Then \log_a corrected for all other extinction was plotted against the air mass. The extintion was 1.76% after 69 iterations (Table III).

Constance of the aerosol size distribution should be calculated at least for a period of 1 h or 2 h. For the calculation of relative aerosol masses a mean aerosol height distribution was used. Bulleit¹⁰ and Hamel¹¹ recorded a strong dependence of aerosol particle size on relative humidity. The variation of the refractive index with relative humidity is calculated at a height of 69 iterations. After 69 iterations the aerosol size distribution is calculated for a given air mass can be calculated air mass zero. From $\log_a(A/A_0) = -u$, the optical depth of aerosols u for a given air mass can be calculated value A_0 can be determined by linear interpolation to plotte against the air mass. The extintion was plotted against the air mass. The extintion was 1.76% after 69 iterations (Table III).